

Article

The Origin of the Caiyuanzi Pb–Zn Deposit in SE Yunnan Province, China: Constraints from In Situ S and Pb Isotopes

Yongguo Jiang ^{1,2}, Yinliang Cui ^{1,2}, Hongliang Nian ², Changhua Yang ², Yahui Zhang ^{3,*}, Mingyong Liu ², Heng Xu ², Jinjun Cai ² and Hesong Liu ³

¹ Faculty of Land Resources Engineering, Kunming University of Science and Technology, Kunming 650093, China

² Yunnan Nonferrous Geological Bureau, Kunming 650051, China

³ Key Laboratory of Critical Minerals Metallogeny in Universities of Yunnan Province, School of Earth Sciences, Yunnan University, Kunming 650500, China

* Correspondence: yahuizh@126.com or zhangyahui@ynu.edu.cn

Abstract: Located at the intersection of the Tethys and Pacific Rim metallogenic belts, the Laojunshan polymetallic metallogenic province in SE Yunnan Province hosts many large-scale W–Sn and Sn–Zn polymetallic deposits. The newly discovered Caiyuanzi medium-sized Pb–Zn deposit is located in the northern part of this province and has eight sulfide ore bodies. All the ore bodies occur in the siliceous rocks of the Lower Devonian Pojiao Formation (D_{1p}). The ore bodies are conformable with stratigraphy and controlled by a lithologic horizon. The sulfide ores have banded or laminated structures. The ore minerals are mainly pyrite, chalcopyrite, sphalerite, and galena. In this study, in situ sulfur and lead isotopes were used to constrain the origin of the Caiyuanzi Pb–Zn deposit. The results show that the in situ $\delta^{34}\text{S}$ values of pyrite, chalcopyrite, and sphalerite range from 0.1‰ to 6.0‰, with an average of 4.7‰. This $\delta^{34}\text{S}$ signature reflects the mixing between magmatic-derived and reduced seawater sulfate sulfur. The in situ Pb isotopes characteristics of pyrite, galena, and sphalerite suggest that the sulfur and lead of ore minerals come from the upper crust. Integrating the data obtained from the studies including regional geology, ore geology, and S–Pb isotope geochemistry, we proposed that the Caiyuanzi Pb–Zn deposit is a hydrothermal deposit formed by sedimentary exhalative and magmatic hydrothermal superimposition.



Citation: Jiang, Y.; Cui, Y.; Nian, H.; Yang, C.; Zhang, Y.; Liu, M.; Xu, H.; Cai, J.; Liu, H. The Origin of the Caiyuanzi Pb–Zn Deposit in SE Yunnan Province, China: Constraints from In Situ S and Pb Isotopes.

Minerals **2023**, *13*, 238. <https://doi.org/10.3390/min13020238>

Academic Editor: Mariko Nagashima

Received: 29 December 2022

Revised: 3 February 2023

Accepted: 5 February 2023

Published: 8 February 2023



Copyright: © 2023 by the authors. Licensee MDPI, Basel, Switzerland. This article is an open access article distributed under the terms and conditions of the Creative Commons Attribution (CC BY) license (<https://creativecommons.org/licenses/by/4.0/>).

Keywords: in situ S and Pb isotopes; the source of ore-forming elements; ore genesis; Caiyuanzi Pb–Zn deposit

1. Introduction

The Laojunshan polymetallic metallogenic province in SE Yunnan Province is located at the intersection of the Tethys and Pacific Rim metallogenic belts. This province hosts many large-scale W–Sn and Sn–Zn polymetallic deposits, such as the Dulong super-large Sn–Zn polymetallic deposit, Xinzhai large-scale Sn polymetallic deposit, and the large-scale Nanyangtian W–Sn deposit. In recent years, one large-scale (Hongshiyuan Pb–Zn) and two medium-sized (Gaji Pb–Zn–Cu polymetallic and Caiyuanzi Pb–Zn) deposits have been discovered in the northern part of the province. The Pb–Zn deposits have a total Pb, Zn, and Cu metal resource of nearly 1.2 million tons, indicating that this province has good prospecting potential for these metals.

At present, the genesis of the Pb–Zn deposits is controversial [1–6], but theories include sedimentary exhalative (SEDEX) [1,2,6], and magmatic hydrothermal origins [3–5]. The main reason for the diversity in genetic views is the lack of understanding of the source of ore-forming materials. In this study, the in situ S and Pb isotopes of sphalerite, galena, pyrite, and chalcopyrite are used to trace the source of metallogenic elements and to discuss the ore genesis of the Caiyuanzi Pb–Zn deposit.

2. Geological Setting

2.1. Regional Geology

The Laojunshan metallogenic province is located at the junction of the Cathaysian, Yangtze, and Indochina blocks (Figure 1a), and in the northern part of the Song Chay metamorphosed dome (Figure 1b). The sedimentary environment in this province is complex and diverse and has experienced multiple periods of large-scale magmatic intrusion [7–11].

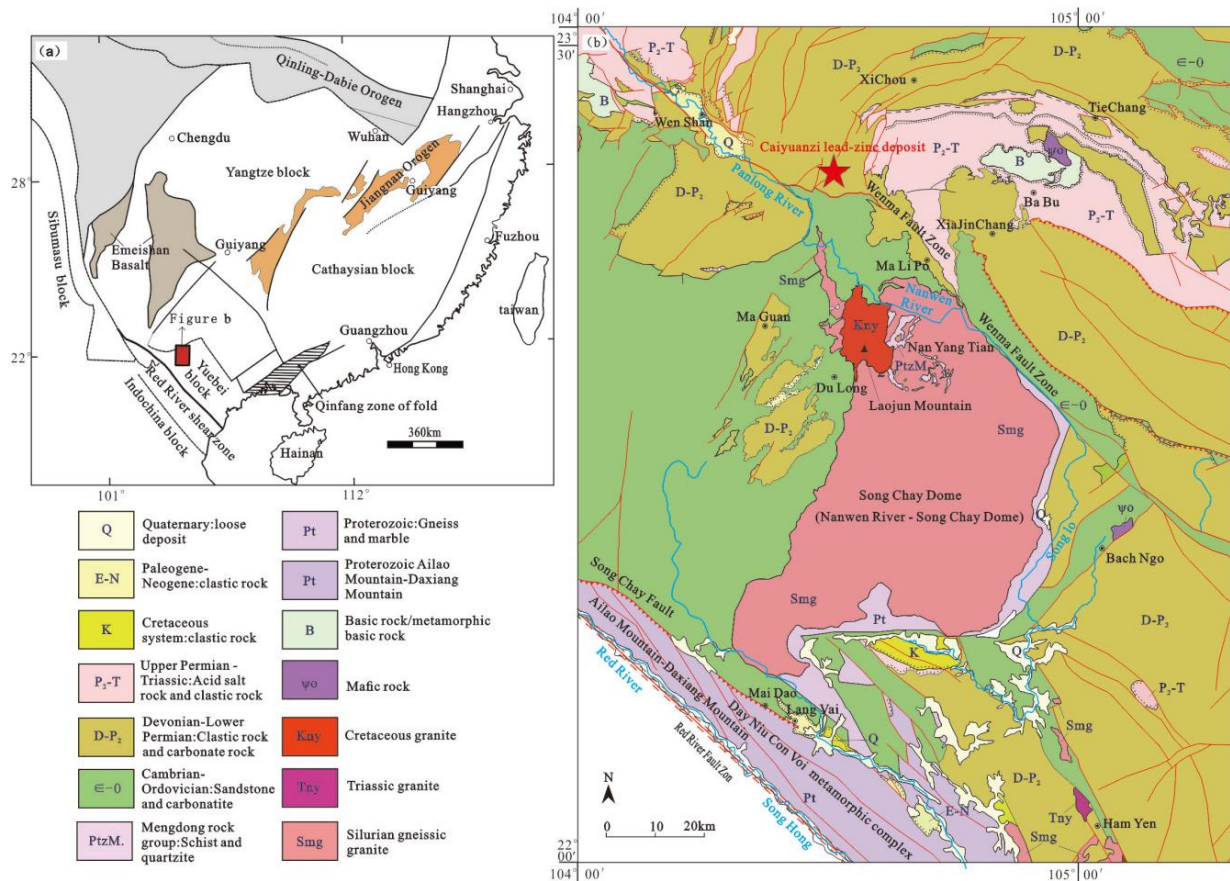


Figure 1. Geotectonic location map of the study area ((a), modified according to [9]) and the regional geological map ((b), quoted from [10]).

Since the Cambrian, this province has experienced repeated transgression and regression, ending in late Triassic marine sedimentation. The exposed strata are Cambrian, Devonian, and Permian, which show a trend of decreasing metamorphism. The Lower Cambrian is mainly sandy argillaceous slate and schist. The abundance of carbonate rocks gradually increases in the upper Middle Cambrian; the Lower Devonian is sandy argillaceous slate, which overlies the Cambrian at a slight angle. The Middle and Upper Devonian are mesa facies carbonate rocks, and the Permian is a continental shelf carbonate with siliceous rocks [12]. There are mainly NNE- and NW-trending regional structures (Figure 1b); the former were formed in the Caledonian–Indosinian, and the latter were formed in the Indosinian–Himalayan [12]. The Nanwenhe and Laojunshan granites are the main igneous rocks, both of which are closely related to tin and zinc polymetallic mineralization in the area [10,13,14]. The Nanwenhe granites are known as the Song Chay granites in the Vietnamese part, and are also known as the Song Chay metamorphic dome [7,8]. They intruded during the late Silurian (420–440 Ma) [7,15,16], and then underwent deformation and metamorphism during the Indosinian, forming gneissic, banded, and eyeball-shaped structures [12]. The Laojunshan granites intruded during the Cretaceous (83–117 Ma) [13,14,17–21].

2.2. Ore Deposit Geology

2.2.1. Strata

The main strata exposed in the mining area are Devonian (Figure 2). The Lower Devonian Pojiao Formation (D_{1p}) comprises shallow continental shelf clastic rocks; the Lower Devonian Gumu Formation (D_{1g}) is a carbonate mesa marginal facies deposit; the Middle Devonian Donggangling Formation (D_{2d}) is a sub-tidal sedimentary of the mesa; the Upper Devonian Gedang Formation (D_{3g}) is a shallow facies carbonate mesa deposit. The Batang Wedge (bw) is an informal stratigraphic unit that belongs to the late Early Devonian–early Middle Devonian carbonate mesa slope facies [22]. The Pojiao Formation is the main ore-hosting layer in the mining area, which is in extensive contact with the overlying Batang Wedge, and has a transitional relationship with the Lower Posongchong Formation. It is mudstone, marl locally interspersed with quartz sandstone, carbonaceous mudstone, marl limestone lens, and has been metamorphosed into mica schist, quartz schist, siliceous dolomite, and locally siliceous rocks.

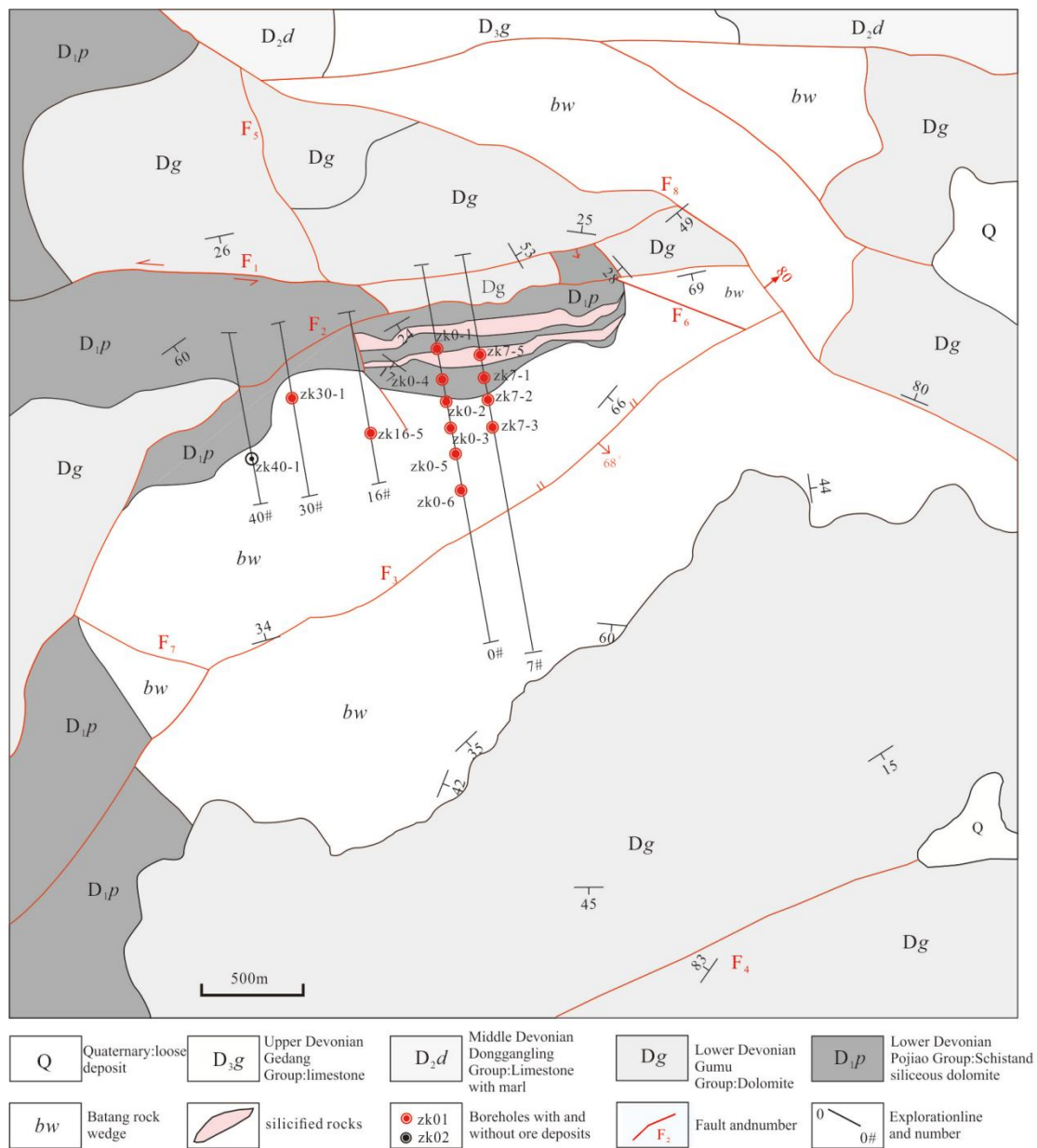


Figure 2. Geological map of mining area.

The Pojiao Formation can be subdivided into two sections [23]. The lower section (D_1p^1) can be divided into three beds from bottom to top, as follows: the first bed is quartz schist and siliceous dolomite; the second is quartz schist mixed with siliceous rocks; the third is carbonaceous mica schist and quartz mica schist. The upper section (D_1p^2) can be divided into four beds from bottom to top, as follows: the first bed is thick bedded siliceous rocks sandwiched between banded quartz schist; the second is quartz schist and siliceous dolomite interspersed with banded siliceous rocks; the third is siliceous dolomite interspersed with siliceous rock; the fourth is quartzite mica schist with quartz schist, locally sandwiched with thin siliceous bands, and locally contains striped pyrite.

2.2.2. Tectonic

The overall structural form of the mining area is a monocline that strikes EW and dips south (Figure 2). A secondary steep slope of compressive tensional NNW, near EW and NE faults developed, off the Xingjie fault (Fs). The strata of the mine area were strongly compressed, resulting in a series of soft wrinkles and folds, which were caused by the above-mentioned fault activity.

2.2.3. Ore Body

A total of eight conformable Pb–Zn strata-bound ore bodies have been found in the mining area, in the siliceous dolomite rocks layer of the Lower Devonian Pojiao Formation (D_1p) (Figure 3). Ores have banded and laminated structures (Figure 4). The main ore body is spread along the banded siliceous dolomite on top of the siliceous rocks [23], which can be divided into lower and upper ore-bearing sections.

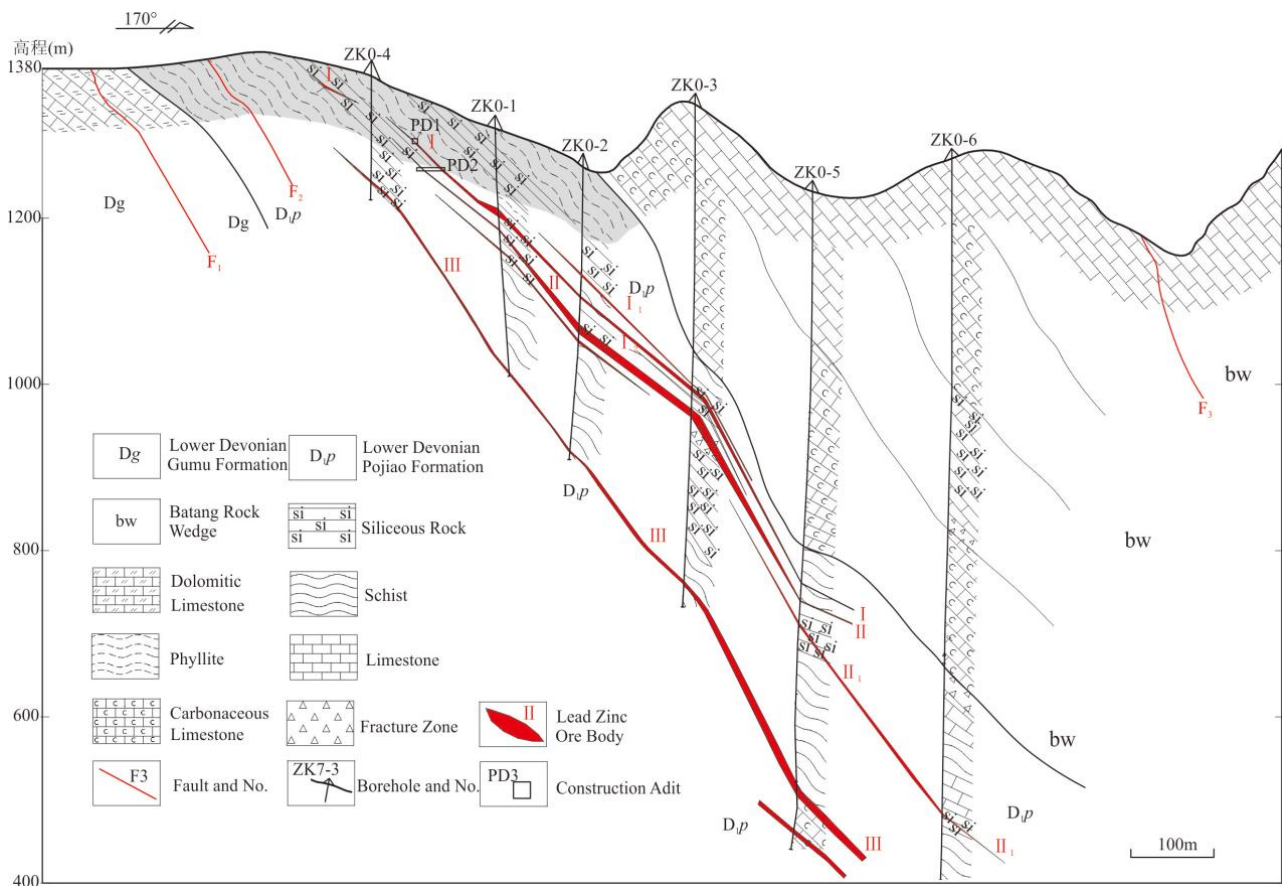


Figure 3. Profile of exploration line 0# in the Caiyuanzi Pb–Zn mining area.

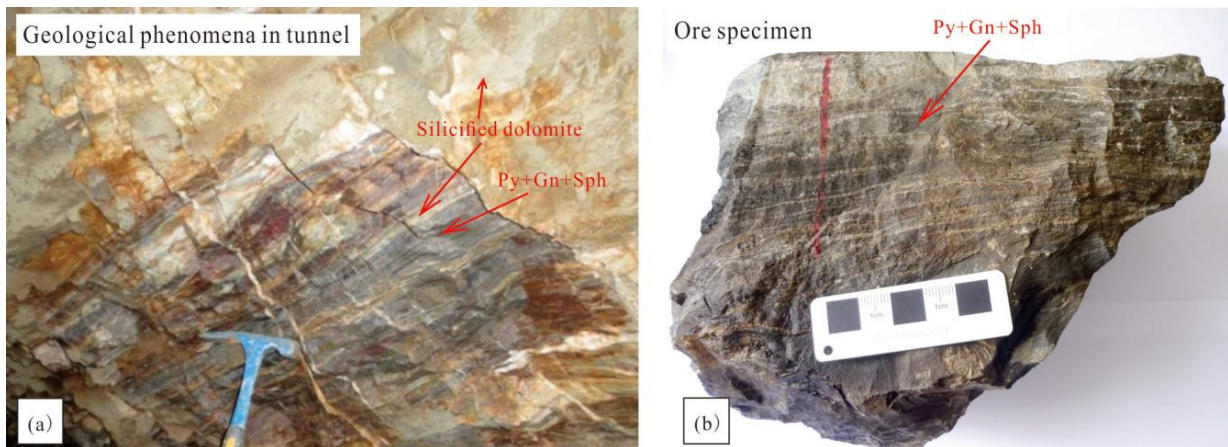


Figure 4. Strata-bound ore body (a) and ores with laminated structure (b). Abbreviations are as follows: Py, pyrite; Gn, galena; Sph, sphalerite.

2.2.4. Texture and Structure

The ore minerals are mainly pyrite, chalcopyrite, sphalerite, and galena, with a small amount of hematite, pyrrhotite, and magnetite, and the gangue minerals are mainly calcite, quartz, and epidote. The ore minerals have euhedral granular, allomorphic granular and metasomatic residual textures. The sulfide ores have massive, disseminated, veined disseminated, banded, and laminated structures (Figure 5).

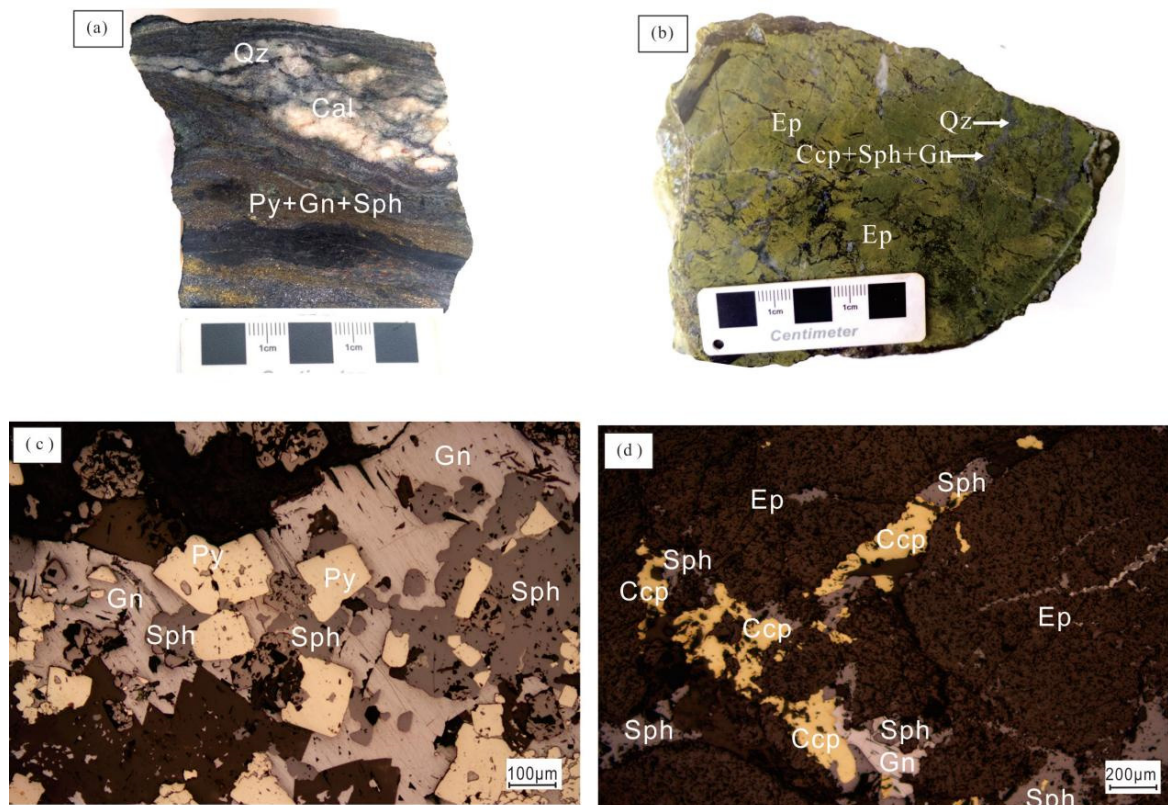


Figure 5. Hand specimens and microscopic photos of the ores from the Caiyuanzi deposit. (a) Disseminated-banded Pb–Zn ore sample (CYZ-1); (b) disseminated-net vein Pb–Zn ore (CYZ-2); (c) pyrite replaced and enclosed by galena and sphalerite; (d) sphalerite, galena, and chalcopyrite, forming network veins occurring along the wall rock fractures, where galena and chalcopyrite alternate with sphalerite. Abbreviations are as follows: Py, pyrite; Gn, galena; Sph, sphalerite; Qz, quartz; Ccp, chalcopyrite; Ep, epidote; Cal, calcite.

The galena, sphalerite, and chalcopyrite are mostly disseminated, veined, banded, and laminated. Pyrite is subhedral to euhedral granular, forming locally fine-grained aggregates; sphalerite and chalcopyrite are anhedral granular and aggregate; galena is allomorphic granular and aggregate. Pyrite is encapsulated and cemented by other sulfides or alternatively metasomatized, suggesting that pyrite formed early. Sphalerite, galena, and chalcopyrite often occur together where galena and chalcopyrite are replaced with sphalerite, indicating that the formation of sphalerite is later than galena and chalcopyrite, but the formation sequence of galena and chalcopyrite is difficult to determine (Figure 5).

2.2.5. Altered Wall Rocks

The wall rock alteration mainly includes silicification, skarnization, pyritization, and calcitization. The wall rock alteration has an enrichment effect on the Pb–Zn–Cu polymetallic mineralization in the mining area. Skarns include actinolite epidote skarn, and chlorite epidote skarn, which are limited to the siliceous limestone in the Pojiao Formation.

3. Sampling and Analytical Methods

3.1. Samples

All the samples were collected from the PD2 tunnel of the Caiyuanzi ore deposit. The detailed information about those samples is listed in Table 1.

Table 1. Information of the samples.

No.	Locations	Features	Purposes
CYZ—1	PD2	Disseminated banded ores	Pb isotope analyses
CYZ—1(1)	PD2	Banded ores	Pb isotope analyses
CYZ—2	PD2	Disseminated ores	S isotope analyses
CYZ—3	PD2	Skarn ores	Pb isotope analyses
CYZ—4	PD2	Sulfide-bearing limestone	
CYZ—5	PD2	Sulfide-bearing calcium siliceous rocks	S and Pb isotope analyses
CYZ—6	PD2	Skarn ores	
CYZ—7	PD2	Sulfide-bearing schistose marble	S isotope analyses

3.2. Analysis Methods

The micro area in situ sulfur isotope test of sulfide was completed in Nanjing Polyspectrum Testing Technology Co., Ltd., and the galena, sphalerite, pyrite, and chalcopyrite of samples CYZ-2, CYZ-5, and CYZ-7 were selected for sulfur isotope analyses. The mass spectrometer model is the Nu Plasma II MC-ICPMS, and the laser model is Analytical Excite. The deep ultraviolet beam generated by the laser generator is focused on the sulfide surface through the homogenizing optical path. First, the gas background is collected for 40 s, and then the appropriate beam spot (pyrite 33 μm ; sphalerite 40 μm ; chalcopyrite 50 μm) at a 5 Hz frequency for 35 s, before the aerosol is sent out of the denudation pool by helium, mixed with argon, and then enters the MC-ICPMS (single integration time is 0.3 s, and there are about 110 groups of data within the denudation time of 35 s). We used a GBW07267 pyrite cake pressed by National Geological Experimental Testing Center of Chinese Academy of Geological Sciences ($\delta^{34}\text{S} = 3.6\text{‰}$) and GBW07268 chalcopyrite cake pressing ($\delta^{34}\text{S} = -0.3\text{‰}$), and NIST SRM 123 crushed zinc blender particles ($\delta^{34}\text{S} = 17.1\text{‰}$) as the data quality control, and the long-term external reproducibility is about $\pm 0.6\text{‰}$ (1 SD).

Micro area in situ lead isotope testing of sulfide was completed in two testing units, respectively. The lead isotope composition analysis of samples CYZ-2 and CYZ-5 was completed in Wuhan Shangpu Analysis Technology Co., Ltd. The instrument model is the MC-ICPMS (Neptune Plus) with multi-receiver mass spectrometry, GeoLas HD with a 193 nm exciter laser ablation system, and a beam spot of 90–120 μm . Energy intensity is 6 mJ/cm^2 , the frequency is 8 Hz, the carrier gas (He) is 500 mL/min, collected data (pulses) are 500, and the recommended values of standard samples (Sph HYLM) are $^{208}\text{Pb}/^{204}\text{Pb}$

(38.519), $^{207}\text{Pb}/^{204}\text{Pb}$ (15.764), and $^{206}\text{Pb}/^{204}\text{Pb}$ (18.217). The lead isotope analyses of samples CYZ-1 and CYZ-3 were completed in the National Key Laboratory of Continental Dynamics, Northwest University. The mass spectrometer model is Nu Plasma II MC-ICPMS, the laser model is Quantronix Integra HE Ti 266 nm NWR UP Femto (ESI, Hartland, WI, USA), and the erosion radius is 15–65 μm . The laser frequency is 5–50 Hz, the erosion mode is 3 $\mu\text{m}/\text{s}$ lines scanning, and the He airflow is 0.7 L/min. The sample standard sample cross method is adopted. The standard sample is NIST610, and the analysis error is better than 0.003 (1 σ).

4. Results

4.1. In Situ S Isotopic Compositions

The results of in situ S isotopic compositions of pyrite, chalcopyrite, and sphalerite are shown in Table 2 and Figure 6. Pyrite, chalcopyrite, and sphalerite have $\delta^{34}\text{S}$ values between 0.1‰ and 6‰, with an average of 4.7‰ (Figure 7). Pyrite has $\delta^{34}\text{S}$ values ranging from 4.3‰ to 6‰ (except 0.1‰ for one point), with an average of 5.40‰; sphalerite has $\delta^{34}\text{S}$ values are between 4.7‰ and 5.3‰, with an average of 5.08‰; chalcopyrite has $\delta^{34}\text{S}$ values are between 4.3‰ and 4.9‰, with an average of 4.67‰.

Table 2. In situ sulfur isotopic compositions of ore sulfides.

No.	Point No.	Mineral	$\delta^{34}\text{S}$ (‰)
cyz-2	cpy-sp-1	Sphalerite	4.70
	cpy-sp-3	Chalcopyrite	4.50
	cpy-sp-4	Chalcopyrite	4.90
	cpy-sp-5	Chalcopyrite	4.90
	py-sp-1	Pyrite	0.10
	py-sp-2	Pyrite	5.00
	py-sp-3	Sphalerite	4.70
	py-sp-4	Pyrite	6.00
cyz-5	cpy-Gn-1	Chalcopyrite	4.70
	cpy-Gn-2	Chalcopyrite	5.10
	pyd-pyx-sp-cpy-1	Pyrite	5.30
	pyd-pyx-sp-cpy-2	Pyrite	5.90
	pyd-pyx-sp-cpy-3	Pyrite	5.50
	pyd-pyx-sp-cpy-4	Sphalerite	4.90
	pyd-pyx-sp-cpy-5	Sphalerite	5.20
	sp-cpy-1	Sphalerite	5.30
sp-cpy-2	Chalcopyrite	4.90	
cyz-7	cpy-1	Chalcopyrite	4.40
	cpy1-1	Chalcopyrite	4.80
	cpy-2	Chalcopyrite	4.30
	cpy-5	Sphalerite	4.30

4.2. In Situ Pb Isotopic Ratios

The results of LA-MC-ICPMS in situ Pb isotopes of galena are listed in Table 3. The Pb isotopic ratios of galena are relatively uniform, with $^{206}\text{Pb}/^{204}\text{Pb}$, $^{207}\text{Pb}/^{204}\text{Pb}$, and $^{208}\text{Pb}/^{204}\text{Pb}$ ratios of 18.134–18.202 (mean 18.158), 15.698–15.735 (mean 15.715), and 38.430–38.542 (mean 38.46), respectively.

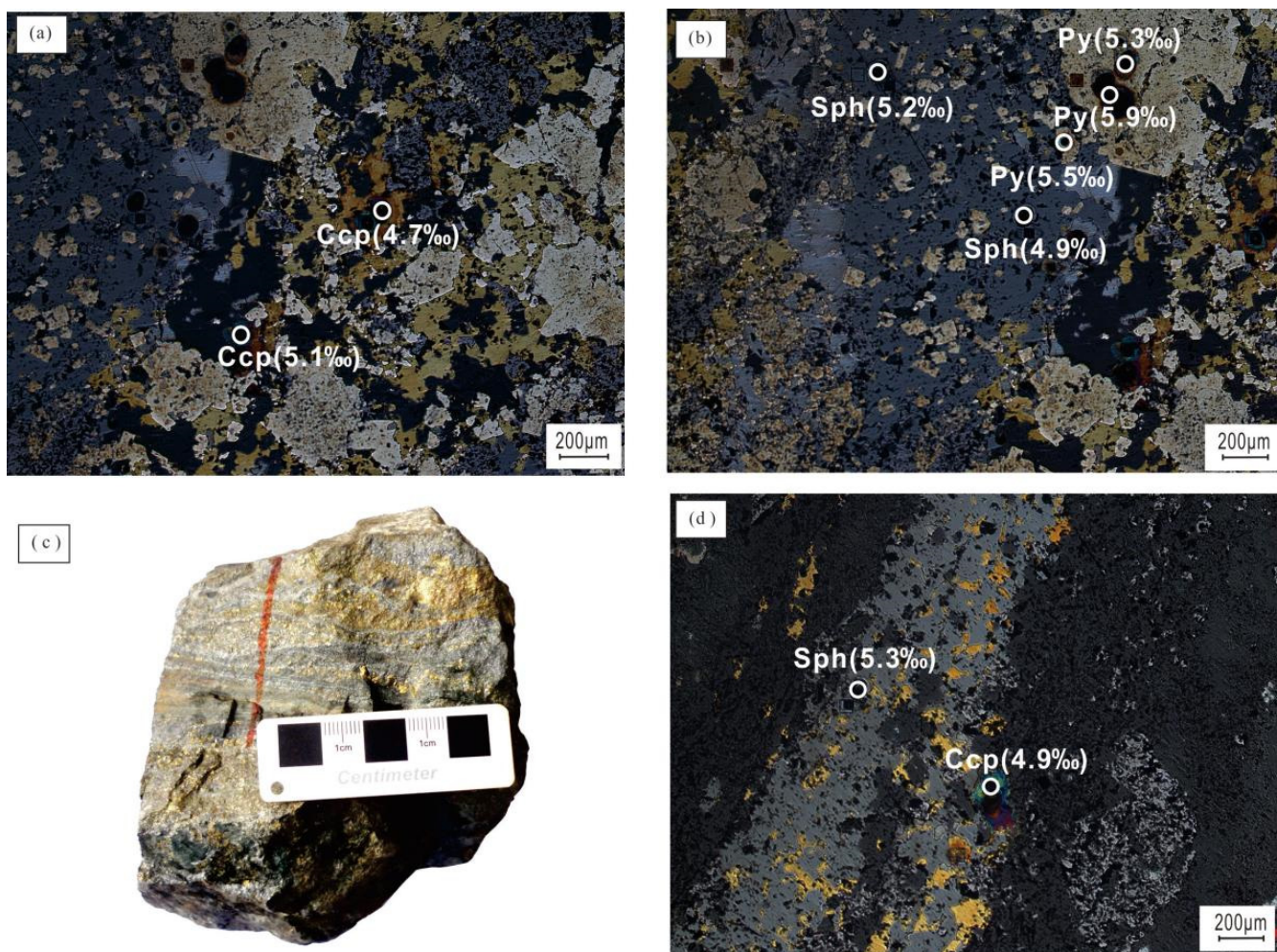


Figure 6. In situ S isotope analyses of the Caiyuanzi deposit. (a,b,d) Microscopic photos of metal sulfide and corresponding in situ sulfur isotope values; (c) in situ S isotope test specimen of sulfide ores.

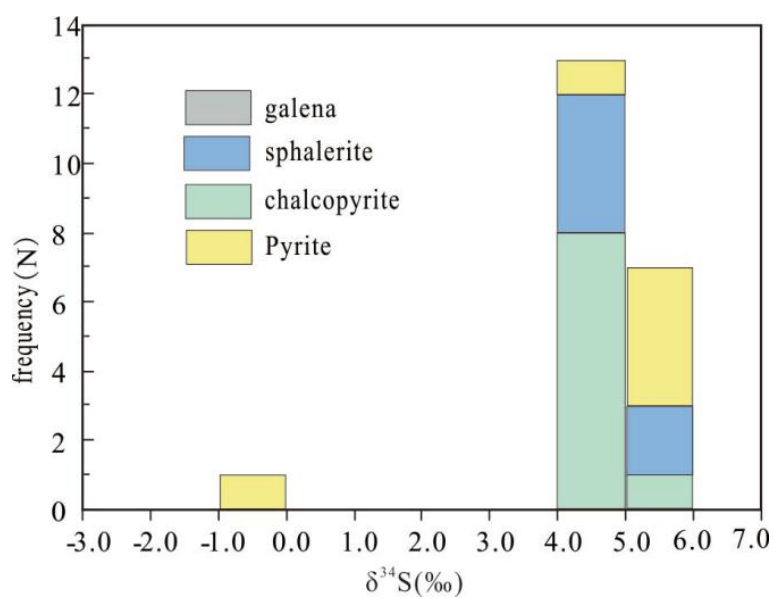


Figure 7. The histogram of S isotopes.

Table 3. In situ Pb isotopes of sphalerite, pyrite, and chalcopyrite.

No.	Deposits	Point Nos.	Mineral	$^{206}\text{Pb}/^{204}\text{Pb}$	1s	$^{207}\text{Pb}/^{204}\text{Pb}$	1s	$^{208}\text{Pb}/^{204}\text{Pb}$	1s		
CYZ-1		GN-1	Galena	18.148	0.001	15.712	0.001	38.449	0.002		
		1-GN-2	Galena	18.146	0.001	15.711	0.001	38.447	0.002		
		1-GN-7	Galena	18.142	0.004	15.707	0.004	38.432	0.010		
		1-GN-8	Galena	18.134	0.001	15.698	0.001	38.410	0.003		
CYZ-1	Caiyuanzi	GN-1	Galena	18.153	0.001	15.719	0.001	38.464	0.002		
		GN-10	Galena	18.147	0.001	15.710	0.001	38.445	0.002		
		GN-11	Galena	18.148	0.001	15.711	0.001	38.444	0.002		
		GN-2	Galena	18.151	0.001	15.717	0.001	38.461	0.002		
		GN-3	Galena	18.153	0.001	15.718	0.001	38.463	0.002		
		GN-4	Galena	18.147	0.001	15.712	0.001	38.449	0.003		
		GN-5	Galena	18.146	0.001	15.711	0.001	38.446	0.002		
		GN-6	Galena	18.145	0.001	15.709	0.001	38.437	0.002		
		GN-7	Galena	18.143	0.001	15.707	0.001	38.435	0.002		
		GN-8	Galena	18.144	0.001	15.708	0.001	38.438	0.002		
CYZ-1	Caiyuanzi	GN-9	Galena	18.142	0.001	15.707	0.001	38.434	0.002		
		SP-1	Sphalerite	18.162	0.022	15.720	0.020	38.473	0.052		
		CYZ-2	Caiyuanzi	01	Pyrite	18.170	0.003	15.728	0.003	38.510	0.006
				04	Pyrite	18.167	0.002	15.721	0.002	38.492	0.006
		CYZ-5	Caiyuanzi	02	Pyrite	18.147	0.006	15.720	0.004	38.467	0.011
		CYZ-3	Caiyuanzi	GN-1	Galena	18.147	0.001	15.703	0.001	38.430	0.003
				GN-10	Galena	18.154	0.001	15.709	0.001	38.444	0.003
				GN-11	Galena	18.151	0.001	15.706	0.001	38.438	0.002
				GN-12	Galena	18.152	0.001	15.708	0.001	38.445	0.002
				GN-2	Galena	18.149	0.001	15.705	0.001	38.436	0.003
GN-3	Galena			18.158	0.001	15.716	0.001	38.468	0.002		
GN-4	Galena			18.158	0.001	15.717	0.001	38.470	0.002		
GN-5	Galena			18.157	0.001	15.716	0.001	38.469	0.003		
GN-6	Galena			18.153	0.001	15.711	0.001	38.455	0.003		
GN-7	Galena			18.151	0.001	15.708	0.001	38.445	0.003		
CYZ-3	Caiyuanzi	GN-8	Galena	18.149	0.001	15.706	0.001	38.443	0.002		
		GN-9	Galena	18.156	0.001	15.711	0.001	38.453	0.002		

5. Discussion

5.1. Source and Formation Mechanism of Reduced Sulfur

Sulfur isotopes are one of the most important bases for determining the source of sulfur and the formation process of sulfide deposits [24–61]. Three sources of sulfur have been proposed, as follows: (1) mantle-derived sulfur, $\delta^{34}\text{S} = -3\text{‰}$ to 3‰ (average 0‰); (2) sedimentary sulfur (marine sulfate), which could form reduced sulfur by thermochemical sulfate reduction (TSR) or bacterial sulfate reduction (BSR) [32,37]; and (3) mixed sulfur of the above two types [31].

The ore mineral assemblages of the Caiyuanzi Pb–Zn deposit are simple, with mainly pyrite, sphalerite, and galena and other sulfides. The $\delta^{34}\text{S}$ values of the Caiyuanzi deposit are relatively homogeneous (0.1‰ to 6‰ , with a mean value of 4.7‰) and positive, which may represent the $\delta^{34}\text{S}_{\Sigma\text{S}}$ of the ore-forming hydrothermal fluids.

The $\delta^{34}\text{S}$ values differ significantly from the values found in typical Mississippi Valley-type (MVT) Pb–Zn deposits, whose reduced sulfur was mainly formed by TSR and/or BSR; for example, the $\delta^{34}\text{S}$ values of sulfides in the Daliangzi (MVT) Pb–Zn deposit are mainly 10‰ to 20‰ [39,41], while the in situ $\delta^{34}\text{S}$ values of sulfides in the Maoping (MVT) Pb–Zn deposit ore are -20.4‰ to 25.6‰ [33,35,40].

In addition, the sulfur isotopic compositions of the Caiyuanzi Pb–Zn deposit are similar to those of the adjacent Gejiu Sn and Dulong Sn–Zn polymetallic deposits (Figure 8), whose sulfur was mainly derived from the magmatic rocks, with less marine sulfate [13,14]. For example, the $\delta^{34}\text{S}$ values of the Gejiu deposit are mainly -3.1‰ to 8.4‰ [51], and the $\delta^{34}\text{S}$

values of the Dulong deposit are mainly 4.2‰ to 12.4‰, most being 5.2‰–9.4‰ [10,42]. Hence, we propose that the sulfur for the Caiyuanzi deposit is mainly derived from the magmatic rocks, although some contribution from the wall rock cannot be excluded.

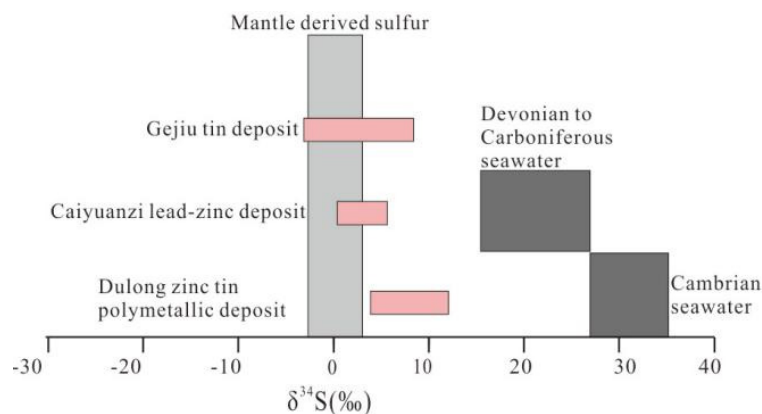


Figure 8. Comparison of sulfur isotopic composition between Pb–Zn deposits in strata of different ages in the Laojunshan region and seawater- and mantle-derived sulfur in the same period (the isotopic composition range of mantle derived sulfur is according to [52]; the sulfur isotopic composition range of seawater in the same period is according to [54]; the sulfur isotopic composition range of ore deposits is according to [10,42,51]).

5.2. Source of Metals

Due to the low contents of U and Th, the proportion of radiogenic Pb in sulfide minerals is negligible. Therefore, Pb isotopes of galena could represent the Pb isotopes of the ore-forming fluids without age correction [49,50]. The in situ Pb isotopic ratios of galena from the Caiyuanzi Pb–Zn deposit obtained in this study has a narrow range (Table 3), suggesting either a single source or a high degree of homogenization in the ore-forming metals in this deposit [39]. In this paper, we collected Pb isotopic data from the Laojunshan granites, marble, schist, and ores in Dulong (Table 3). The samples of the Caiyuanzi deposit fall on the average upper crustal growth curve and mantle curve in the corresponding Figure 9a,b, respectively. The whole rock Pb isotope ratios of marble and schist are significantly different from those of the Caiyuanzi deposit (Figure 9), so the wall rocks (marble and schist) may not have provide lead to the deposit. The data of Yanshanian granites are concentrated between the orogenic belt and the upper crust, close to the upper crust, and its $^{208}\text{Pb}/^{204}\text{Pb}$ and $^{207}\text{Pb}/^{204}\text{Pb}$ ratios are consistent with the data of Caiyuanzi sample points. The Pb isotope ratios of the Caiyuanzi and Dulong deposits and the Yanshanian granites have the same distribution range and trend and are projected between the orogenic belt and the upper crustal evolution curve, indicating that the Laojunshan granites might have provided metals for the Caiyuanzi deposit. Another end member should be the underlying Proterozoic rocks, with relatively unradiogenic crustal Pb.

In addition, the μ values ($^{238}\text{U}/^{204}\text{Pb}$) of the Caiyuanzi deposit range from 9.71 to 9.76, which are between the mantle or lower crust Pb ($\mu = 7.86\text{--}7.94$) and upper crust Pb ($\mu = 9.81$), and so could be a mixture between them. The average value of ω is 39.14, which is closer to the upper crust Pb between normal lead ($\omega = 35.55 \pm 0.59$) and the upper crust Pb (41.860) [38]. The Th/U average value is 3.89, which is close to normal Pb (Th/U = 3.92 ± 0.9), slightly higher than the upper crust of the Chinese mainland (Th/U = 3.76). In the corresponding Pb isotope $\Delta\beta\text{--}\Delta\gamma$ genetic classification diagram [55], the data point of the Caiyuanzi deposit falls in the upper crust Pb source area (Figure 10).

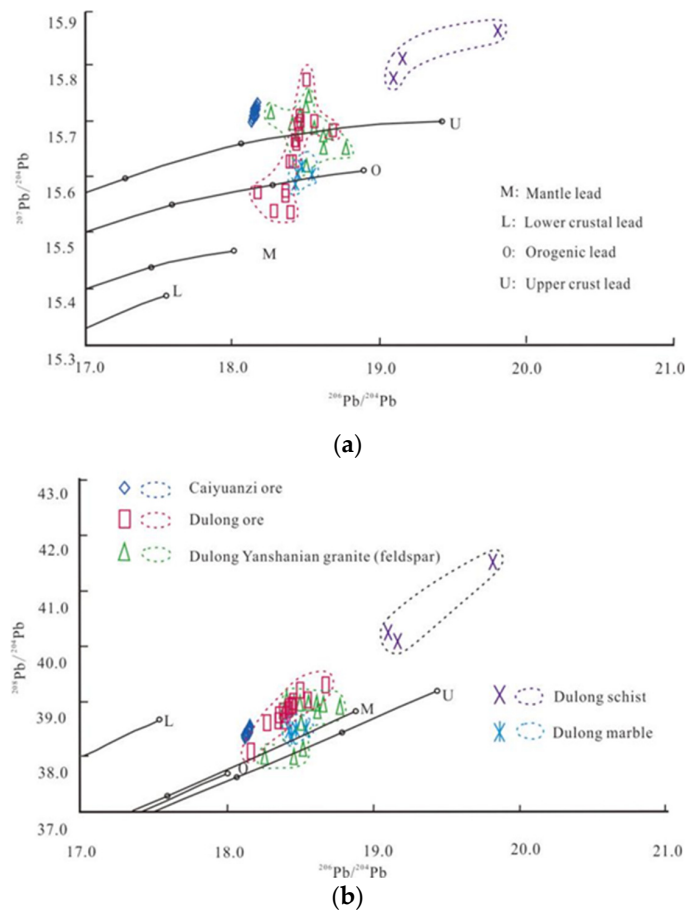


Figure 9. The Pb model diagram for the Caiyuanzi deposit (base map is modeled after [38,62], and lead isotope data of samples in the Dulong ore area are quoted from [43]). (a) The samples of the Caiyuanzi deposit fall on the average upper crustal growth curve. (b) The mantle curve in the corresponding.

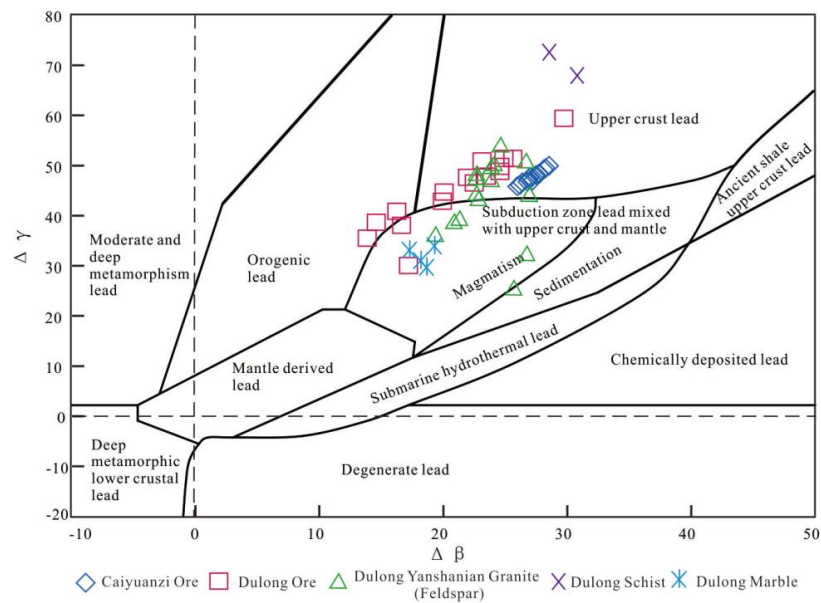


Figure 10. Lead isotope $\Delta\beta$ - $\Delta\gamma$ genetic classification diagram (base map is modeled after [55], and lead isotope data of samples in the Dulong ore area are quoted from [43]).

The Pb isotopes of the Dulong deposit and the Yanshanian granites span two source areas of upper crustal Pb and magmatic Pb, and generally show a trend from magmatic Pb to crustal Pb, suggesting that the intermediate-acidic magma rich in deep-source low μ -value Pb has been contaminated by shallow-source high μ -value Pb during ascent. The μ values of the Dulong deposit (9.56) and the Dulong Yanshanian granites ($\mu = 9.62$) are similar to that of the Caiyuanzi deposit ($\mu = 9.72$).

The degree of crustal contamination of magmatic hydrothermal fluids is positively correlated with the μ values [44], suggesting that the intermediate-acid magmatic hydrothermal fluids related to the Caiyuanzi Pb–Zn deposit are greatly contaminated by crustal materials. In addition, the Pb isotope of sulfides in the Caiyuanzi deposit is significantly higher in U/Pb ($^{208}\text{Pb}/^{204}\text{Pb} > 18.000$, $^{207}\text{Pb}/^{204}\text{Pb} > 15.300$), and slightly lower in Th/Pb ($^{208}\text{Pb}/^{204}\text{Pb} < 39.000$), suggesting that the ore-forming material is dominated by upper crust lead, with a small amount of deep crust-derived magmatic Pb, showing the characteristics of orogenic belt Pb.

5.3. Ore Genesis

At present, the ore genesis of the Pb–Zn deposits in the Laojunshan area is still controversial. The focus is whether it belongs to a SEDEX deposit or a magmatic hydrothermal deposit. In this paper, the in situ S and Pb isotopes of the Caiyuanzi Pb–Zn deposit show that the sulfur was mainly derived from the mixed sources of magmatic rocks and marine sulfate, and the source of metal Pb is the upper crust. The ore bodies are strata-bound and stratiform, which resembles the SEDEX deposits (Table 4). However, the Caiyuanzi Pb–Zn deposit is characterized by epigenetic mineralization with extensive pyrrhotite and skarnization, which can be compared to the general metallogenic characteristics of magmatic hydrothermal deposits. Most of ore bodies and ores underwent some fractures and deformation. Therefore, all of these observations suggest that the Caiyuanzi Pb–Zn deposit was a product of syn-sedimentary hydrothermal exhalative and superimposed magmatic–hydrothermal ore-forming processes.

Table 4. Summary and comparison of principal characteristics of SEDEX, MVT, magmatic hydrothermal vein-type, and the Caiyuanzi Pb–Zn deposit.

Features	Sedimentary Exhalative (SEDEX)	Mississippi Valley-Type (MVT)	Magmatic Hydrothermal Vein-Type	Caiyuanzi Deposit
Ore-forming age	Syngenetic—early diagenetic	Epigenetic	Epigenetic	Syngenetic, epigenetic
Geological setting	Extensional first and second-order basins	Carbonate platform sequences and thrust belts, rare occurrences in extensional basins	Varied	Thrust belt
Host rocks	Varied. Mainly sandstones, siltstones, limestones, dolomites, cherts, and turbidites	Limestones, dolostones, and rare micrites	Varied. Sandstone, siltstone, and carbonates	Siliceous dolomite, quartz schist
Structural controls	Syn-sedimentary faults controlling sub-basins and associated fractures and breccias	Normal, trans-tensional, and wrench faults and associated fractures and breccias	Fault zone/strata	Lithologic interface
Associated igneous activity	No direct association with igneous activity, but tuffs related to synchronous distal volcanism may be present	Not associated with igneous activity	Associated with igneous activity	Associated with igneous activity
Ore-body morphology	Single or multiple wedge- or lens-shaped, or sheeted/stratiform morphology	Commonly discordant on a deposit scale but strata-bound on a regional scale	Veins, stratiform-like morphology	Stratiform-like morphology

Table 4. Cont.

Features	Sedimentary Exhalative (SEDEX)	Mississippi Valley-Type (MVT)	Magmatic Hydrothermal Vein-Type	Caiyuanzi Deposit
Mineralogy	Sp, Gn, and Py (\pm Pyr) and common Brt, Ap, and very rare Fl	Sp, Gn, Py, Mar, minor Dol, Cal, Fl (rare), Cpy, and Brt (minor to absent)	Sp, Gn, Py, Cpy, and minor Brt	Sp, Gn, Py, Ccp, minor Hem, Po, Mag, Grt, and Chl
Host rock alteration	Silicification, chloritization, epidotization, albitization	Carbonatization, silicification	Silicification, pyritic and carbonate alteration	Silicification, skarnization
References	[56]	[57–59]	[60,61]	This paper

Abbreviations are as follows: Sp, sphalerite; Gn, galena; Py, pyrite; Brt, barite; Ap, apatite; Cpy, chalcocopyrite; Fl, fluorite; hem, hematite; Po, pyrrhotite; Mag, magnetite, Grt, garnet, Chl, chlorite.

In South China, the Devonian is widely exposed and consists of carbonate and clastic deposition of large transgressive-regressive cycles [63]. The Devonian sedimentary rocks in South China host numerous SEDEX pyrite deposits, such as Dajiangping [64], and sedimentary reworking deposits, such as Huodehong [65]. The reducing environment within the early Devonian sea floor led to the rapid burial of organic matter. The reduction of marine sulfate by organic matter formed S^{2-} and then mixed with deeply-derived Pb and Zn, etc., and eventually formed the syn-sedimentary sulfide ore bodies. During the Cretaceous, extensional tectonics developed in South China. The southeastern Yunnan–northern Guangxi and the large-scale mineralization in Late Mesozoic in western South China were controlled by a similar continental dynamic background [48]. After 135 Ma, the movement direction of the Izanagi plate in eastern China changed, from the subduction of the Eurasian continent to rapid strike-slip along a NE direction [46], and the South China region underwent lithospheric extension. As a result of the extension of the lithosphere, the lithospheric mantle has undergone underplating and upwelling, resulting in a large amount of ferromagnesian magmatism. Upwelling of this magma and underplating of the lower crust, as well as the partial melting of the lower crust, may have produced granitic melt that invaded the upper crust [45]. During this period, a large number of granite bodies were formed in southeastern Yunnan, such as the Gejiu, Laojunshan, and Bozhushan granites. At the same time, a number of world-class W–Sn polymetallic deposits related to granites were formed, such as the Gejiu, Dulong, Dachang, and Bainiuchang deposits. The newly obtained S and Pb isotopic data from Caiyuanzi suggest that the mineralization is related to the Yanshanian granites in Laojunshan. The regional magmatic hydrothermal events contributed to the Dulong Sn (diopside, garnet, and tremolite skarn) and Zn mineralization (epidote skarn, although some parts show a lack of skarn minerals), and Caiyuanzi skarnization (epidote, garnet skarn).

6. Conclusions

- (1) The sulfur and lead of ore minerals come from the upper crust and mantle.
- (2) The Caiyuanzi Pb–Zn deposit is a hydrothermal deposit formed by the superimposed magma of sedimentary exhalative.

Author Contributions: Investigation, Y.J. and Y.Z.; writing–original draft preparation, Y.J.; writing–review and editing, H.N., C.Y., M.L., H.X., J.C. and H.L.; supervision, Y.C. and Y.Z.; funding acquisition, Y.Z. All authors have read and agreed to the published version of the manuscript.

Funding: This research was financially supported by the National Natural Science Foundation of China (No. 41802087) and the Basic Research Program of Yunnan Provincial Department of Science and Technology, China (No. 2019FB144).

Data Availability Statement: The data used to support this study are included within the article.

Acknowledgments: The field work was supported and assisted by workers of the No. 317 Geological Teams of Yunnan Nonferrous Geological Bureau. The experimental process was guided and assisted by the staff of the two laboratories. We would like to express our heartfelt thanks to them! We sincerely thank the Editorial Board members and anonymous reviewers for their constructive comments.

Conflicts of Interest: The authors declare that they have no known competing financial interest or personal relationships that could have appeared to influence the work reported in this paper.

References

1. Lin, Q.S. Geological characteristics and Ore-hunting Significance of the Hongshiyian Jets sedimentary Type lead-zinc-copper deposits in Xichou County, Yunnan Province. *Fujian Geol.* **2013**, *32*, 185–192.
2. Li, Z.Q.; Huan, J.G.; Han, R.S.; Ren, T.; Wang, L.; Qiu, W.L. Geochemical Characteristics and Tectonic Setting of Epidote Rocks from in the Hongshiyian Pb-Zn-Cu Polymetallic Ore Deposit, Southeastern Yunnan Province. *Geol. Explor.* **2013**, *49*, 289–299.
3. Yang, C.B.; Pu, C.; Shi, G.F.; Wang, Y.Z.; Yang, F.X.; Zheng, T.P.; Zhang, X.H. The feature and prospecting criteria of Gaji Pb-Zn Deposit in Xichou, Yunnan. *Yunnan Geol.* **2020**, *39*, 1–7.
4. Yang, C.B.; Pu, C.; Wang, Y.Z.; Shi, G.F.; Yang, F.X.; Zheng, T.P.; Zhang, X.H. Mineralization characteristics of the Gaji Cu-Pb-Zn polymetallic deposit, Xichou County, Yunnan Province, China. *Acta Mineral. Sin.* **2020**, *40*, 255–266.
5. Ma, Y.H.; Wang, J.S.; Yu, W.X.; Yang, C.B.; Zheng, X.J.; Han, H.H.; He, H. Zircon U-Pb geochronology and Hf isotopic characteristics of metamorphic rocks in the Gaji polymetallic metallogenic area in the southeastern Yunnan and their geological implications. *Acta Mineral. Sin.* **2021**, *41*, 129–140.
6. Cai, J.J.; Wang, J.D.; Li, L.X.; Yang, Z. The feature and genesis of Caiyuanzi Pb-Zn-Cu Deposit in Xichou, Yunnan. *Yunnan Geol.* **2021**, *40*, 193–198.
7. Roger, F.; Leloup, P.H.; Jolivet, M.; Lacassin, R.; Trinh, P.T.; Brunel, M.; Seward, D. Long and complex thermal history of the Song Chay metamorphic dome (Northern Vietnam) by multi-system geochronology. *Tectonophysics* **2000**, *321*, 449–466. [[CrossRef](#)]
8. Maluskia, H.; Lepvrier, C.; Jolivet, L.; Carter, A.; Roques, D.; Beyssac, O.; Trong, T.T.; Duc, T.N.; Avigad, D. Ar-Ar and fission-track ages in the Song Chay Massif: Early Triassic and Cenozoic tectonics in northern Vietnam. *J. Asian Earth Sci.* **2001**, *19*, 233–248. [[CrossRef](#)]
9. Yang, J.H.; Cawood, P.A.; Du, Y.S.; Huang, H.; Hu, L.S. Detrital record of Indosinian mountain building in SW China: Provenance of the Middle Triassic turbidites in the Youjiang Basin. *Tectonophysics* **2012**, *574–575*, 105–117. [[CrossRef](#)]
10. Niu, H.B. *The Ore-Forming Fluid and Metallogenesis of W-Sn Polymetallic Deposits in the Nanwenhe-Song Chay Dome Areas, Southeastern Yunnan Province*; Guangzhou Institute of Geochemistry, Chinese Academy of Sciences: Guangzhou, China, 2021.
11. Mei, M.X.; Li, Z.Y. Sequence Stratigraphic Succession and Sedimentary Basin Evolution from Late Paleozoic to Triassic in Yunnan-Guizhou-Guangxi Region. *Geoscience* **2004**, *18*, 555–563.
12. Zhang, S.T.; Feng, M.G.; Lv, W. Analysis of the Nanwenhe Metamorphic Core Complex in Southeast Yunnan. *Regional Geol. China* **1998**, *17*, 390–397.
13. Liu, Y.P.; Li, Z.X.; Li, H.M.; Guo, L.G.; Xu, W.; Ye, L.; Li, C.Y.; Pi, D.H. U-Pb geochronology of cassiterite and zircon from the Dulong Sn-Zn deposit: Evidence for Cretaceous large-scale granitic magmatism and mineralization events in southeastern Yunnan province, China. *Acta Petrol. Sin.* **2007**, *23*, 967–976.
14. Xu, B.; Jiang, S.Y.; Wang, R. Late Cretaceous granites from the giant Dulong Sn-polymetallic ore district in Yunnan Province, South China: Geochronology, geochemistry, mineral chemistry and Nd-Hf isotopic compositions. *Lithos* **2015**, *218–219*, 54–72. [[CrossRef](#)]
15. Carter, A.; Roques, D.; Bristow, C.; Kinny, P. Understanding Mesozoic accretion in Southeast Asia: Significance of Triassic thermotectonism (Indosinian orogeny) in Vietnam. *Geology* **2001**, *29*, 211–214. [[CrossRef](#)]
16. Guo, L.G.; Liu, Y.P.; Li, C.Y.; Xu, W.; Ye, L. SHRIMP zircon U-Pb geochronology and litho-geochemistry of Caledonian Granites from the Laojunshan area, south eastern Yunnan province, China: Implications for the collision between the Yangtze and Cathaysia blocks. *Geochem. J.* **2009**, *43*, 101–122. [[CrossRef](#)]
17. Feng, J.R.; Mao, J.W.; Pei, R.F.; Zhou, Z.H.; Yang, Z.X. SHRIMP zircon U-Pb dating and geochemical characteristics of Laojunshan granite intrusion from the Wazha tungsten deposit, Yunnan Province and their implications for petrogenesis. *Acta Petrol. Sin.* **2010**, *26*, 845–857.
18. Zhang, B.H.; Ding, J.; Ren, G.M.; Zhang, L.K.; Shi, H.Z. Geochronology and Geochemical Characteristics of the Laojunshan Granites in Maguan County, Yunnan Province, and Its Geological Implications. *Acta Geol. Sin.* **2012**, *86*, 587–601.
19. Feng, J.R.; Mao, J.W.; Pei, R.F. Ages and geochemistry of Laojunshan granites in southeastern Yunnan, China: Implications for W-Sn polymetallic ore deposits. *Mineral. Petrol.* **2013**, *107*, 573–589. [[CrossRef](#)]
20. Liu, Y.B.; Mo, X.X.; Zhang, D.; Que, C.Y.; Di, Y.J.; Pu, X.M.; Cheng, G.S.; Ma, H.H. Petrogenesis of the Late Cretaceous granite discovered in the Laojunshan region, southeastern Yunnan Province. *Acta Petrol. Sin.* **2014**, *30*, 3271–3286.
21. Lan, J.B.; Liu, Y.P.; Ye, L.; Zhang, Q.; Wang, D.P.; Su, H. Geochemistry and age spectrum of Late Yanshanian granites from Laojunshan Area, Southeastern Yunnan Province, China. *Acta Mineral. Sin.* **2016**, *36*, 477–491.

22. The Second Geological Brigade of Yunnan Provincial Bureau of Geological and Mineral Exploration and Development. *Regional Geological Survey Report of 1/50000 Xingjie Street*; The Second Geological Brigade of Yunnan Provincial Bureau of Geological and Mineral Exploration and Development: Wenshan, China, 1995.
23. Hunan Tiangong Mining Technology Co., Ltd. *Detailed Geological Survey Report of Ganshapo Lead Zinc (Copper) Mine in Xichou County, Yunnan Province*; Hunan Tiangong Mining Technology Co., Ltd.: Changsha, China, 2014.
24. Cheng, Y.S.; Sun, W.M. Sulfur and lead isotope geochemistry of the Dulong Sn-Zn polymetallic ore deposit, Yunnan province, China. *Nonferrous Met.* **2019**, *71*, 32–36, 65.
25. Guo, Y.W.; Zhang, Q.S.; Zhu, P.B.; Lu, D.; Wang, N.; Ai, J.B. Study on sulphur and lead isotope composition characteristics and ore material source of Wanlongshan Sn-Zn polymetallic ore deposit in Yunnan province. *Contrib. Geol. Min. Res.* **2018**, *33*, 564–572.
26. He, F.; Zhang, Q.; Wang, D.P.; Liu, Y.P.; Ye, L.; Bao, T.; Wang, X.J.; Miao, Y.L.; Zhang, S.K.; Su, H.; et al. Ore-Forming Materials Sources of the Dulong Sn-Zn Polymetallic Deposit, Yunnan, Evidences from S-C-O Stable Isotopes. *Bull. Min. Petrol. Geochem.* **2014**, *33*, 900–907.
27. Ohmoto, H. Systematics of sulfur and carbon isotopes in hydrothermal ore deposits. *Econ. Geol.* **1972**, *67*, 551–578. [[CrossRef](#)]
28. Ohmoto, H. Stable isotope geochemistry of ore deposit. *Rev. Mineral.* **1986**, *16*, 491–559.
29. Zhou, J.X.; Wang, X.C.; Wilds, S.A.; Luo, K.; Huang, Z.L.; Wu, T.; Jin, Z.G. New Insights into the Metallogeny of MVT Zn-Pb Deposits: A Case Study from the Nayongzhi in South China, Using Field Data, Fluid Compositions, and In-Situ S-Pb Isotopes. *Am. Mineral.* **2018**, *103*, 91–108. [[CrossRef](#)]
30. Machel, H.G.; Krouse, H.R.; Sassen, R. Products and distinguishing criteria of bacterial and thermochemical sulfate reduction. *Appl. Geochem.* **1995**, *10*, 373–389. [[CrossRef](#)]
31. Tan, S.C.; Zhou, J.X.; Zhou, M.F.; Ye, L. In-situ S and Pb isotope constraints in an evolving hydrothermal system, Tianbaoshan Pb-Zn-(Cu) deposit in South China. *Ore Geol. Rev.* **2019**, *115*, 103177. [[CrossRef](#)]
32. Seal, R.R. Sulfur isotope geochemistry of sulfide minerals. *Rev. Mineral. Geochem.* **2006**, *61*, 633–677. [[CrossRef](#)]
33. Tan, S.C.; Zhou, J.X.; Luo, K.; Xiang, Z.Z.; He, X.H.; Zhang, Y.H. The sources of ore-forming elements of the Maoping large-scale Pb-Zn deposit, Yunnan Province: Constrains from in-situ S and Pb isotopes. *Acta Petrol. Sin.* **2019**, *35*, 3461–3476.
34. Basuki, N.; Taylor, B.E.; Spooner, E.T.C. Sulfur isotope evidence for thermochemical reduction of dissolved sulfate in Mississippi Valley-type zinc-lead mineralization, Bongara area, northern Peru. *Econ. Geol.* **2008**, *103*, 783–799. [[CrossRef](#)]
35. Zhou, J.X.; Xiang, Z.Z.; Zhou, M.F.; Feng, Y.X.; Luo, K.; Huang, Z.L.; Wu, T. The giant upper Yangtze Pb-Zn province in SW China: Reviews, new advances and a new genetic model. *J. Asian Earth Sci.* **2018**, *154*, 280–315. [[CrossRef](#)]
36. Zheng, Y.F.; Chen, J.F. *Stable Isotope Geochemistry*; Science Press: Beijing, China, 2000.
37. Shanks, W.C. Stable isotopes in seafloor hydrothermal systems: Vent fluids, hydrothermal deposits, hydrothermal alteration, and microbial processes. *Rev. Min. Geochem.* **2001**, *43*, 469–525. [[CrossRef](#)]
38. Doe, B.R.; Zartman, R.E. *Geochemistry of Hydrothermal Ore Deposits*; John Wiley & Sons: New York, NY, USA, 1979.
39. Huang, Z.L.; Chen, J.; Han, R.S.; Li, W.B.; Liu, C.Q.; Zhang, Z.L.; Ma, D.Y.; Gao, D.R.; Yang, H.L. *Geochemistry and Genesis of the Huize Super-Large Lead-Zinc Deposit in Yunnan Province—A Discussion on the Relationship between the Emeishan Basalt and Lead-Zinc Mineralization*; Geological Publishing House: Beijing, China, 2004.
40. Ren, S.L.; Li, Y.H.; Zeng, P.S.; Qiu, W.L.; Fan, C.F.; Hu, G.Y. Effect of Sulfate Evaporate Salt Layer in Mineralization of the Huize and Maoping Lead-Zinc Deposits in Yunnan: Evidence from Sulfur Isotope. *Acta Geol. Sin.* **2018**, *92*, 1041–1055.
41. Zhou, J.X.; Huang, Z.L.; Zhou, M.F.; Zhu, X.K.; Mucchez, P. Zinc, sulfur and lead isotopic variations in carbonate-hosted Pb-Zn sulfide deposits, Southwest China. *Ore Geol. Rev.* **2014**, *58*, 41–54. [[CrossRef](#)]
42. Liu, Y.P.; Li, C.Y.; Gu, T.; Wang, J.L. Isotopic constraints on the source of ore-forming materials of Dulong Sn-Zn polymetallic deposit, Yunnan. *Geol. Geochem.* **2000**, *28*, 75–81.
43. He, F.; Zhang, Q.; Liu, Y.P.; Ye, L.; Miao, Y.L.; Wang, D.P.; Su, H.; Bao, T.; Wang, X.J. Lead Isotope Compositions of Dulong Sn-Zn Polymetallic Deposit, Yunnan, China: Constraints on Ore-forming Metal Sources. *Acta Mineral. Sin.* **2015**, *35*, 309–317.
44. Yang, Y.L.; Ye, L.; Cheng, Z.T.; Bao, T.; Gao, W. A tentative discussion on the genesis of skarn Pb-Zn deposits in the Baoshan-Zhenkang terrane. *Acta Petrol. Mineral.* **2012**, *31*, 554–564.
45. Bergantz, G.W. Underplating and partial melting: Implications for melt generation and extraction. *Science* **1989**, *245*, 1093–1095. [[CrossRef](#)]
46. Mao, J.W.; Wang, Y.T.; Li, H.M.; Piraino, F.; Zhang, C.Q.; Wang, R.T. The relationship of mantle-derived fluids to gold metallogenesis in the Jiaodong Peninsula: Evidence from D-O-C-S isotope systematics. *Ore Geol. Rev.* **2008**, *33*, 361–381. [[CrossRef](#)]
47. Chen, Y.Q.; Huang, J.N.; Lu, Y.X.; Xia, Q.L.; Sun, M.X.; Li, J.R. Geochemistry of Elements, Sulphur-Lead Isotopes and Fluid Inclusions from Jinla Pb-Zn-Ag Poly-Metallic Ore Field at the Joint Area across China and Myanmar Border. *J. Earth Sci.* **2009**, *34*, 585–594.
48. Cheng, Y.B.; Mao, J.W.; Chen, X.L.; Li, W. LA-ICP-MS Zircon U-Pb Dating of the Bozhushan Granite in Southeastern Yunnan Province and Its Significance. *J. Jilin Univ.* **2010**, *40*, 869–878.
49. Carr, G.R.; Dean, J.A.; Suppel, D.W.; Heithersay, P.S. Precise lead isotope fingerprinting of hydrothermal activity associated with Ordovician to Carboniferous metallogenic events in the Lachlan fold belt of New South Wales. *Econ. Geol.* **1995**, *90*, 1467–1505. [[CrossRef](#)]
50. Zhou, J.X.; Yang, Z.M.; An, Y.L.; Luo, K.; Liu, C.; Ju, Y. An evolving MVT hydrothermal system: Insights from the Niujiatong Cd-Zn ore field, SW China. *J. Asian Earth Sci.* **2022**, *237*, 105357. [[CrossRef](#)]

51. Cheng, Y.B.; Mao, J.W. *Study on Diagenesis and Mineralization in Gejiu Super Large Tin Polymetallic Ore Concentration Area, Yunnan*; Geological Publishing House: Beijing, China, 2014.
52. Chaussidon, M.; Albarède, F.; Sheppard, S.M.F. Sulphur isotope variations in the mantle from ion microprobe analyses of micro-sulphide inclusions. *Earth Planet. Sci. Lett.* **1989**, *92*, 144–156. [[CrossRef](#)]
53. Ohmoto, H.; Goldhaber, M.B. *Sulfur and Carbon Isotopes*, 3rd ed.; John Wiley & Sons: New York, NY, USA, 1997.
54. Claypool, G.E.; Holser, W.T.; Kaplan, I.R.; Sakai, H.; Zak, I. The age curves of sulfur and oxygen isotopes in marine sulfate and their mutual interpretation. *Chem. Geol.* **1980**, *28*, 199–260. [[CrossRef](#)]
55. Zhu, B.Q. *Theories and Application of Isotopic System in Geoscience: Crustal and Mantle Evolution in China Continent*; Science Press: Beijing, China, 1998; pp. 1–330. (In Chinese with English Abstract).
56. Leach, D.L.; Sangster, D.F.; Kelley, K.D.; Large, R.R.; Garven, G.; Allen, C.R. Sediment-hosted Pb-Zn Deposits: A global perspective. *Econ. Geol.* **2005**, *100*, 561–608.
57. Leach, D.L.; Bradley, D.C.; Huston, D.; Pisarevsky, S.A.; Taylor, R.D.; Gardoll, S.J. Sediment-hosted lead-zinc deposits in Earth history. *Econ. Geol.* **2010**, *105*, 593–625. [[CrossRef](#)]
58. Luo, K.; Zhou, J.X.; Huang, Z.L.; Caulfield, J.; Zhao, J.X.; Feng, Y.X.; Ouyang, H. New insights into the evolution of Mississippi Valley-Type hydrothermal system: A case study of the Wusihe Pb-Zn deposit, South China, using quartz in-situ trace elements and sulfides in situ S-Pb isotopes. *Am. Mineral.* **2020**, *105*, 35–51. [[CrossRef](#)]
59. Luo, K.; Zhou, J.X.; Huang, Z.L.; Wang, X.C.; Wilde, S.A.; Zhou, W.; Tian, L. New insights into the origin of early Cambrian carbonate-hosted Pb-Zn deposits in South China: A case study of the Maliping Pb-Zn deposit. *Gondwana Res.* **2019**, *70*, 88–103. [[CrossRef](#)]
60. Wang, C.; Zhang, D.; Wu, G.; Santosh, M.; Zhang, J.; Xu, Y.; Zhang, Y. Geological and isotopic evidence for magmatic-hydrothermal origin of the Ag-Pb-Zn deposits in the Lengshuikeng District, east-central China. *Miner. Depos.* **2014**, *49*, 733–749. [[CrossRef](#)]
61. Zhou, Z.; Wen, H.; Qin, C.; Liu, L. Geochemical and isotopic evidence for a magmatic-hydrothermal origin of the polymetallic vein-type Zn-Pb deposits in the northwest margin of Jiangnan Orogen, South China. *Ore Geol. Rev.* **2017**, *86*, 673–691. [[CrossRef](#)]
62. Zartman, R.E.; Doe, B.R. Plumbotectonics: The model. *Tectonophysics* **1981**, *75*, 135–162. [[CrossRef](#)]
63. Ma, X.P.; Liao, W.H.; Wang, D.M. *The Devonian System of China, with a Discussion on Sea-Level Change in South China*; Geological Society of London Special Publication: London, UK, 2009; Volume 314, pp. 241–262.
64. Qiu, W.J.; Zhou, M.F.; Li, X.; Williams-Jones, A.E.; Yuan, H. The genesis of the giant Dajiangping SEDEX-type pyrite deposit, South China. *Econ. Geol.* **2018**, *113*, 1419–1446. [[CrossRef](#)]
65. Luo, K.; Zhou, J.X.; Sun, G.T.; Nguyen, A.; Qin, Z.X. The metallogeny of the Devonian sediment-hosted sulfide deposits, South China: A case study of the Huodehong deposit. *Ore Geol. Rev.* **2022**, *143*, 104747. [[CrossRef](#)]

Disclaimer/Publisher’s Note: The statements, opinions and data contained in all publications are solely those of the individual author(s) and contributor(s) and not of MDPI and/or the editor(s). MDPI and/or the editor(s) disclaim responsibility for any injury to people or property resulting from any ideas, methods, instructions or products referred to in the content.